# Biomimetic metal-mediated reactivity

Wegeberg, Christina

Chapter 3 – Paper I

# Halogen-Bonding-Assisted Iodosylbenzene Activation by a Homogenous Iron Catalyst

**Activation through halogen-bonding**: Stabilization of an iron(III)–OIPh complex in the gas, solution, and solid phases is ascribed to strong intermolecular halogen-bonding. Two molecules of an iron(III) complex with a hexadentate ligand are proposed to work in unison to break the polymeric structure of $[PhIO]_n$, concomitantly solubilizing and activating it to give a system that efficiently catalyzes the selective oxidation of electron-rich substrates.

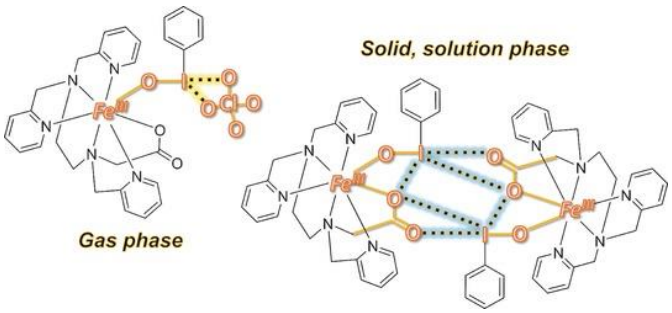


This chapter has been published as
D. P. de Sousa, C. Wegeberg, Mads S. Vad, S. Mørup, C. Frandsen, W. A. Donald, C. J. McKenzie
*Chem. Eur. J.* **2016**, *22*, 3810 – 3820
The supporting information can be found on https://doi.org/10.1002/chem.201503112

ChemPubSoc Europe
DOI: 10.1002/chem.201503112
CHEMISTRY A European Journal Full Paper

Halogen Bonding

# Halogen-Bonding-Assisted Iodosylbenzene Activation by a Homogenous Iron Catalyst

David P. de Sousa,[a] Christina Wegeberg,[a] Mads Sørensen Vad,[a] Steen Mørup,[b] Cathrine Frandsen,[b] William A. Donald,[c] and Christine J. McKenzie*[a]

**Abstract:** The iron(III) complex of hexadentate *N*,*N*,*N*′-tris(2-pyridylmethyl)ethylendiamine-*N*′-acetate (tpena$^-$) is a more effective homogenous catalyst for selective sulfoxidation and epoxidation with insoluble iodosylbenzene, $[PhIO]_n$, compared with soluble methyl-morpholine-*N*-oxide (NMO). We propose that two molecules of $[Fe(tpena)]^{2+}$ cooperate to solubilize PhIO, extracting two equivalents to form the halogen-bonded dimeric $\{[Fe(tpena)OIPh]_2\}^{4+}$. The closest intradimeric I···O distance, 2.56 Å, is nearly 1 Å less than the sum of the van de Waals radii of these atoms. A correlation of the rates of the reaction of $\{[Fe(tpena)OIPh]_2\}^{4+}$ with *para*-substituted thioanisoles indicate that this species is a direct metal-based oxidant rather than a derived ferryl or perferryl complex. A study of gas-phase reactions indicate that an ion at $m/z = 231.06100$ originates from solution-state $\{[Fe(tpena)OIPh]_2\}^{4+}$ and is ascribed to $[Fe^{III}(tpenaO)]^{2+}$, derived from an intramolecular O atom insertion into an Fe–tpena donor bond. Proposed ion pairs, $\{[Fe(tpena)OIPh]Cl\}^+$ and $\{[Fe(tpena)OIPh]ClO_4\}^+$, are more stable than native $[Fe(tpena)OIPh]^{2+}$ ions, suggesting that halogen-bonding, as for the solution and solid states, operates also in the gas phase.

## Introduction

The hypervalent iodine compound, iodosylbenzene (PhIO), is a convenient oxidant because it is easy to prepare and a relatively stable solid. It suffers disadvantages, however, with respect to implementation in homogenous catalysis owing to its general insolubility. Efforts to overcome this have included functionalizing the benzene group with solubilizing sulfonate groups.[1] In an alternative approach, we have communicated that the iron(III) complex of the carboxylato-containing hexadentate ligand, *N*,*N*,*N*′-tris(2-pyridylmethyl)ethylendiamine-*N*′-acetate (tpena$^-$), not only aids PhIO solubilization but also catalyzes the selective sulfoxidation of thioanisole.[2] This reaction is interesting as the oxidant is provided, as needed, during the course of the reaction: Thus, substrates are not potentially deleteriously exposed to large amounts of excess oxidant and selectivity is enhanced. Our initial observations suggest that this system is amongst the most efficient in terms of rates for catalytic systems utilizing PhIO as terminal oxidant, despite the heterogeneity.

Tpena$^-$ is a potentially hexadentate chelating ligand. In this respect, it would seem at face value that the property of open coordination sites, for enabling reactant(s) and product coordination, possibly simultaneously, is challenged. The X-ray crystal structure of the as yet unique iron(III)–OIPh adduct, $[Fe(tpena)OIPh](ClO_4)_2$,[2] shows, however, that the iron(III) is seven-coordinated. Although hepta-coordination is common for high-spin iron(III), this geometry is sometimes overlooked in catalytic mechanisms proposed for synthetic catalysts and enzymes alike. Similar to other iron(III)-terminal oxidant adducts (superoxo,[3] peroxo,[4] hydroperoxo,[5] alkylperoxo,[6] hypochlorite[7]), iodosylaryls[2,8] have been variously proposed as the direct catalytically competent iron and manganese-based oxidants; however, unlike the aforementioned superoxo and peroxo adducts, there is no general consensus for the assignment of the salient spectroscopic fingerprints for metal–OIPh adducts. The present work most inconveniently divulges few salient features for recognizing this important moiety. It does, however, shed light on the way in which iron(III) complexes can activate insoluble PhIO.

The use of PhIO as a terminal oxidant is not generally perceived as desirable within the paradigms of green chemistry. This situation is only worsened if soluble derivatives need to be used. Thus, a strategy of employing a metal complex to both labilize and activate PhIO, as described here, has merits. Not only is the issue of solubility resolved, the presence of an excess of solubilized oxidant in the solution is also avoided. This will reduce the risk of the ubiquitous side-products often

[a] D. P. de Sousa, C. Wegeberg, Dr. M. S. Vad, Prof. C. J. McKenzie
Department of Physics, Chemistry and Pharmacy
University of Southern Denmark, Campusvej 55, 5230 Odense M (Denmark)
E-mail: mckenzie@sdu.dk

[b] Prof. S. Mørup, Prof. C. Frandsen
Department of Physics, Technical University of Denmark
DK-2800, Kongens Lyngby (Denmark)

[c] Dr. W. A. Donald
School of Chemistry, University of New South Wales
Sydney, NSW (Australia)

Supporting information for this article is available on the WWW under http://dx.doi.org/10.1002/chem.201503112.

Part of a Special Issue "Women in Chemistry" to celebrate International Women's Day 2016. To view the complete issue, visit: http://dx.doi.org/chem.v22.11.

ChemPubSoc Europe

CHEMISTRY A European Journal Full Paper

observed in catalytic oxidation chemistry. An environmentally friendly system for recycling PhIO from the cleanly generated side-product PhI would be very interesting with respect to potential applications for the efficient and selective catalytic oxidation reactions.

## Results and Discussion

The most convenient starting material for the chemistry described here is the oxo-bridged $[Fe_2(\mu\text{-}O)(tpenaH)_2](ClO_4)_4$ (**1**$(ClO_4)_4$).[2] By dissolving **1**$(ClO_4)_4$ in non-aqueous solvents (acetonitrile, acetone), pseudo-dehydration [Eq. (1)] effects oxo-bridge cleavage to give $[Fe(tpena)]^{2+}$ (**2**). In this process, two uncoordinated protonated pendant pyridines are deprotonated and the oxo bridge is concurrently protonated to form water. This takes approximately 15 min at room temperature, whereupon the color of the solution changes from yellow–brown to red (Figure S2 in the Supporting Information).

$$[Fe_2O(tpenaH)_2]^{4+}\ (\mathbf{1}) \rightleftharpoons 2\ [Fe(tpena)]^{2+}\ (\mathbf{2}) + H_2O \quad Eq.\ 1$$

By adding/diffusing diethyl ether at −40°C into solutions of **2**, solid and hygroscopic [Fe(tpena)]$(ClO_4)_2$ (**2**$(ClO_4)_2$) can be isolated in powder and/or crystalline forms. The powders appear to be lighter orange in color compared with the red–orange crystals—more than can be warranted by particle size differences. IR and Mössbauer spectroscopy (see below) show that the bulk powder and crystalline products are mixtures of **2**$(ClO_4)_2$ and **1**$(ClO_4)_4$. Photos of the red–orange crystals of **2**$(ClO_4)_2$ show that they are dispersed with crystals of its brown pseudo-hydrate, **1**$(ClO_4)_4$ (Figure S1 in the Supporting Information). Complex **2** can be expected to exist as *fac*-$py_3$ ($\mathbf{2}^{fac}$; py = pyridine) and *mer*-$py_3$ ($\mathbf{2}^{mer}$) isomers (Figure 1) and the dehydration of **1** [Eq. (1)] can potentially yield both. In contrast to in the X-ray crystal structure of **1**, $tpena^-$ has fully realized its potential as a hexadentate ligand in the X-ray crystal structure obtained for the red–orange crystals of $\mathbf{2}^{fac}$ (Figure 1, Tables S1 and S2 in the Supporting Information). The iron(III)–donor bonds are all less than 2 Å. When compared to iron(III) complexes with as close as possible N5O coordination,[9] this would seem consistent with a low-spin ($S = 1/2$) d-electron configuration. The relatively close intermolecular interactions and a Fe···Fe distance of 6.078(1) Å between pairs of dicationic $\mathbf{2}^{fac}$ is notable. This seems to suggest a strong association through non-classic hydrogen-bonding in short intradimer α-pyCH···O interactions involving the coordinated and non-coordinated carboxylato O atoms and π–π stacking of pyridines, which can overcome the coloumbic repulsions between the dications of $\mathbf{2}^{fac}$. Four counter anions and acetonitrile solvate surround the dimer. It is relevant to note that the closest intermolecular M···M distances in cobalt(III)[10] and chromium(III)[11] analogues are longer (8.844 Å and 7.517 Å) and there is no such distinctly obvious pairing in the solid state.

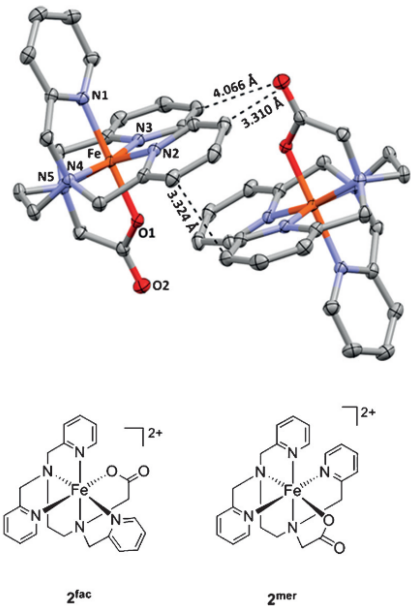





$\mathbf{2}^{fac}$ $\mathbf{2}^{mer}$

**Figure 1.** The associated cations of $\mathbf{2}^{fac}$ in the X-ray crystal structure of [Fe(tpena)]$(ClO_4)_2(CH_3CN)_{0.5}$ and chemical diagrams of the *fac*-$py_3$ ($\mathbf{2}^{fac}$) and *mer*-$py_3$ ($\mathbf{2}^{mer}$) geometrical isomers. Displacement ellipsoids are drawn at the 50% probability level.

### Strong halogen-bonding enables isolation of an intrinsically unstable PhIO complex

If solid PhIO is added to dry acetonitrile solutions containing **2**, an immediate color change from red to orange is seen, which is indicative of the formation of $[Fe(tpena)OIPh]^{2+}$ (**3**), which can be isolated as its perchlorate salt by rapid precipitation on addition of diethyl ether at −40°C. We have previously communicated the X-ray crystal structure of **3**$(ClO_4)_2$.[2] A comparison of the conformations of $tpena^-$ in $\mathbf{2}^{fac}$ and **3** suggests that the direct solution-state precursor for **3** is most likely the non-structurally characterized $\mathbf{2}^{mer}$ isomer as the PhIO is inserted *cis* to the three pyridines and the carboxylato ligands are more or less *trans* to the two amine N atoms; this forms the seven-coordinated iron(III) center in **3**. The supramolecular halogen-bonded association of pairs of dicationic complexes that are evident in the X-ray crystal structure have not been previously described (Figure 2). The iron atoms in the dimers are separated by 8.011(1) Å and the closest intermolecular I···O distance is 2.555(3) Å. At 0.94 Å less than the sum of the van der Waals radii of the respective atoms (3.50 Å[12]), this distance indicates very strong halogen-bonding. As depicted, the other intermolecular I···O interactions are also well below 3.5 Å. For reference, the energy of a single I···O halogen-bond between iodobenzene and DMSO has been calculated to be about 3 kcal $mol^{-1}$.[13] The cumulative power of six such close supramolecular intradimer halogen-bonded contacts clearly achieves the stability needed for the crystallization of **3**, which is otherwise

ChemPubSoc Europe

CHEMISTRY
A European Journal
Full Paper



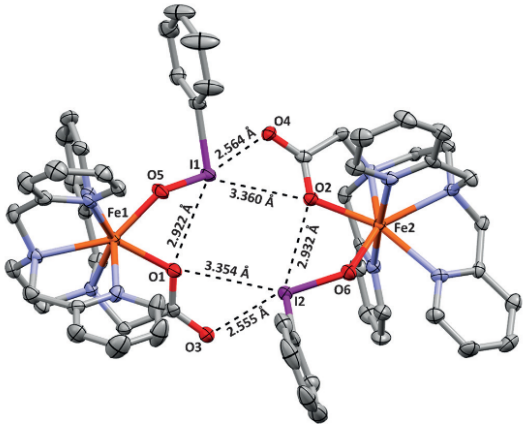


**Figure 2.** Halogen-bonded dimer formation in the X-ray crystal structure of dicationic $[\mathbf{3}]_2$ showing intermolecular I···O distances. Displacement ellipsoids are drawn at the 50% probability level.

expected to be highly reactive. Solid-state samples are stable for months to years at −40 °C. PhIO and its soluble (e.g., sulfonated) derivatives have been used to prepare iron(IV), manganese(V), chromium(V) and cobalt(IV) high-valent metal–oxo complexes[14] by oxygen atom transfer [Eq. (2)]; however, the putative intermediate metal–OIPh species in these systems have not been isolated. This could suggest that in most cases metal complexes of PhIO are more reactive than the derivative higher-valent metal–oxo products. In turn, this balance will determine which of the metal-based oxidants, [LM=O] or [LM–OIPh], are pertinent in the catalysis of oxidation reactions using PhIO as the terminal oxidant in metal-catalyzed reactions.

$$[LM^{n+}] + OIAr \rightleftharpoons [LM^{n+}OIAr] \rightleftharpoons [LM^{(n+2)-}O] + IAr \qquad Eq.\ 2$$

The dimeric associations found in the solid state of $\mathbf{2}^{fac}$ and **3**, along with the fast reaction between **2** and insoluble PhIO, could point towards cooperativity between two molecules of **2** to break the polymeric structure of PhIO to form the unexpectedly relatively robust **3**. The question arises: do the halogen-bonded dimers of **3** observed in the solid state remain intact in solution? When $\mathbf{3}(ClO_4)_2$ is dissolved in non-protic solvents, its half-life, as measured by the disappearance of a shoulder at approximately 430 nm in the UV/Vis spectrum, depends strongly on the solvent. For example, the half-life of **3** decreases in the order of acetonitrile > acetone > nitromethane with $\tau_{1/2}$ values of 4.6, 3.6, and 0.25 h, respectively (Figure S3, Table S3 in the Supporting Information). Thus, the relative stability of **3** in solution correlates with the decreasing acidity of these non-protic solvents. In accordance, **3** cannot exist in protic solvents, presumably because protons will outcompete halogen-bonding for the non-coordinated carbonyl oxygen atoms.

### Dimerization quenches carboxylato vibrations

The IR spectrum of $[PhIO]_n$(s) contains bands at 440, 491, and 595 $cm^{-1}$. In $^{18}O$-labeled $[PhI^{18}O]_n$(s), these are shifted to 414, 482, and 564 $cm^{-1}$, respectively (Figure S4 in the Supporting Information). These are absent in the IR spectrum of $\mathbf{3}(ClO_4)_2$(s) (Figure 3). Weak bands at 684 and 654 $cm^{-1}$ are probably associated with the coordinated PhIO; however, these bands were not shifted in $^{18}O$-labeled samples of **3** prepared by using $PhI^{18}O$. A very weak unassigned band at 470 shifts to 453 $cm^{-1}$ in the spectrum of $^{18}O$-labeled $\mathbf{3}(ClO_4)_2$ (Figure S5 in the Supporting Information). Thus, the unique solid-state metal–OIPh complex $\mathbf{3}(ClO_4)_2$ does not reveal any particularly distinctive IR features that might be used as markers for identifying metal-coordinated PhIO. There is no doubt that the label is present; however, if the $^{18}O$-labeled $\mathbf{3}(ClO_4)_2$ is dissolved in acetonitrile containing one equivalent of thioanisole, this is oxidized and $^{18}O$-labeled methyl phenyl sulfoxide is produced (Figure S9 in the Supporting Information). Similarly inconvenient, there are (surprisingly) no distinctive salient features that distinguish $\mathbf{2}(ClO_4)_2$(s) and $\mathbf{3}(ClO_4)_2$(s) by IR spectroscopy and particularly conspicuous in the spectra of both compounds is the absence or low intensity of the tpena$^-$-derived carboxylate stretches at $\nu_{as(COO)}$ = 1661 $cm^{-1}$ and $\nu_{s(COO)}$ = 1340 $cm^{-1}$. These bands would normally be expected to dominate the spectra of complexes of carboxylato ligands, and are typically used to determine the coordination mode. These stretches are the most intense in the spectrum of $\mathbf{1}(ClO_4)_4$. A low intensity feature at 1661 $cm^{-1}$ in the spectra of $\mathbf{2}(ClO_4)_2$ and $\mathbf{3}(ClO_4)_2$, originating from unavoidable contamination by $\mathbf{1}(ClO_4)_4$, was variable from sample to sample. This is backed up by traces of the absorption band at 837 $cm^{-1}$ assigned to the $\nu_{as(Fe\text{-}O\text{-}Fe)}$ stretch, which is shifted to 771 $cm^{-1}$ when labeled with $^{18}O$ (Figure S6 in the Supporting Information). The unexpected quenching of $\nu_{as(COO)}$ in $\mathbf{2}(ClO_4)_2$(s) and $\mathbf{3}(ClO_4)_2$(s) is attributed to solid-state dimer formation with strong intermolecular interactions between the dications in both structures (Figures 1 and 2).[15] This generates a pseudo-inversion center resulting in the carboxylato groups

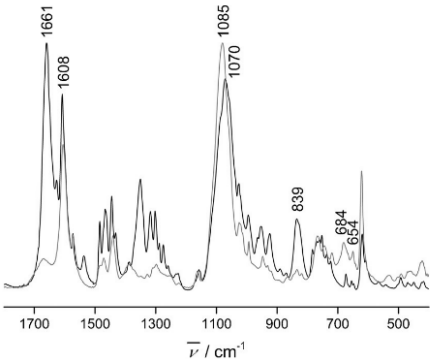


**Figure 3.** IR spectra of $[\mathbf{3}(ClO_4)_2]_2$ (gray) and $\mathbf{1}(ClO_4)_4$ (black).

ChemPubSoc Europe

CHEMISTRY A European Journal Full Paper

becoming symmetrically equivalent and thereby lowering the intensity of the formally IR active $\nu_{as(COO)}$.

### Mössbauer spectroscopy

Mössbauer spectra of bulk powdered samples containing **2**$(ClO_4)_2$ and **3**$(ClO_4)_2$ are shown in Figure 4. Consistent with

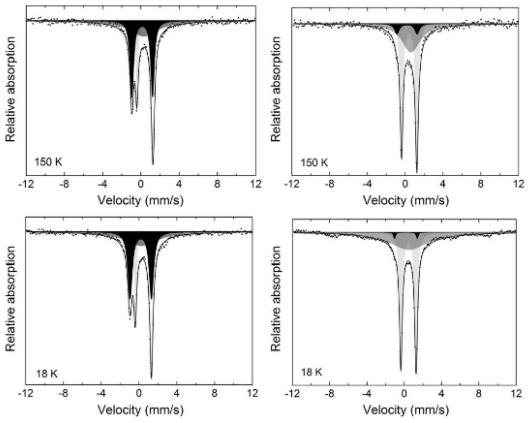


**Figure 4.** Solid-state Mössbauer spectra at 18 K (bottom) and 150 K (top) of solid samples containing the reactive high-spin iron(III) complexes. Left: **2**$^{mer}(ClO_4)_2$ (dark gray). Right: **3**$(ClO_4)_2$ (medium gray). Both samples contain significant contamination by **1**$(ClO_4)_4$ (light gray) and **2**$^{fac}(ClO_4)_2$ (black).

the IR spectra and the equilibrium in Equation (1), both samples show a significant and unavoidable fraction of **1**$(ClO_4)_4$ and **2**$^{fac}(ClO_4)_2$. The Mössbauer parameters assigned to **1**$(ClO_4)_4$,[16] the *fac* and *mer* isomers of **2**$(ClO_4)_2$ (Table 1), and **3**$(ClO_4)_2$ (Table 2) were extracted from fits to both spectra. The broad singlet in the spectrum in Figure 4 (left) was assigned **2**$^{mer}(ClO_4)_2$, which we propose to be high-spin ($S=5/2$), and the one doublet is assigned to low-spin ($S=1/2$) **2**$^{fac}(ClO_4)_2$. Thus, Mössbauer data support the low-spin electronic configuration implied by the bond lengths and the arrangement of the three $\pi$-acceptor pyridine ligands *trans* to the weak-field carboxylato and amine donors in the X-ray crystal structure of

**Table 1.** Mössbauer parameters derived from the solid-state spectrum in Figure 4 a for co-precipitated species **1**, **2**$^{fac}$, and **2**$^{mer}$.[18]

| | $\delta$ [mm s$^{-1}$] | $\Delta E_Q$ [mm s$^{-1}$] | FWHM[a] [mm s$^{-1}$] | $T$ [K] | Assignment | Rel. area [%] |
|---|---|---|---|---|---|---|
| **1**$(ClO_4)_4$ | 0.46 | 1.71 | 0.33 | 18 | high-spin | 25 |
| light gray | 0.44 | 1.72 | 0.33 | 150 | iron(III) | 25 |
| **2**$^{fac}(ClO_4)_2$ | 0.18 | 2.26 | 0.55 | 18 | low-spin | 41 |
| black | 0.14 | 2.16 | 0.44 | 150 | iron(III) | 40 |
| **2**$^{mer}(ClO_4)_2$ | 0.25 | n.a. | 4.19 | 18 | high-spin | 34 |
| dark gray | 0.30 | n.a. | 3.66 | 150 | iron(III) | 35 |

[a] Full width at half maximum.

**Table 2.** Mössbauer parameters derived from the solid-state spectrum in Figure 4 b for co-precipitated **1**, **2**$^{fac}$, and **3**.[18]

| | $\delta$ [mm s$^{-1}$] | $\Delta E_Q$ [mm s$^{-1}$] | FWHM [mm s$^{-1}$] | $T$ [K] | Assignment | Rel. area [%] |
|---|---|---|---|---|---|---|
| **1**$(ClO_4)_4$ | 0.45 | 1.63 | 0.36 | 18 | high-spin | 49 |
| light gray | 0.42 | 1.62 | 0.34 | 150 | iron(III) | 50 |
| **2**$^{fac}(ClO_4)_2$ | 0.18 | 2.43 | 0.25 | 18 | low-spin | 2 |
| black | 0.19 | 2.14 | 0.59 | 150 | iron(III) | 8 |
| **3**$(ClO_4)_2$ | 0.48 | n.a. | 4.94 | 18 | high-spin | 49 |
| medium gray | 0.61 | n.a. | 2.38 | 150 | iron(III) | 43 |

**2**$^{fac}(ClO_4)_2$. This arrangement produces a more symmetrical electronic configuration compared with the anticipated ligand conformation of **2**$^{mer}$ for which a high-spin ($S=5/2$) electronic configuration would be reasonable. A $S=5/2$ electronic configuration for seven-coordinate **3** can be expected and this is consistent with the broad singlet observed in the spectrum (Figure 4, right). Broad singlets are commonly observed for high-spin iron(III) compounds with relatively long paramagnetic relaxation times of the order of a nanosecond.[17] The paramagnetic relaxation can have contributions from temperature-independent spin–spin relaxation and temperature-dependent spin–lattice relaxation. The line width decreases with increasing temperature (Tables 1 and 2), indicating a decrease in the relaxation time. In Figure 4 (right), a broad sextet with low intensity and with a hyperfine field of about 51 T is visible at 18 K, indicating high-spin iron(III) with a relaxation time on the order of several nanoseconds. This weak component was not included in the fit. At 80 K it was not visible. This suggests that it has transformed to a broad singlet because of the faster spin–lattice relaxation at 80 K.

### Solution spectroscopy: PhIO and NMO adducts

The electron spin resonance (ESR) spectrum of **3** in frozen acetonitrile shows an isotropic signal at $g_{iso}=4.50$ consistent with a high-spin ($S=5/2$) electronic configuration persisting in solution (Figure 5 b). If allowed to stand for several hours at room temperature, a rhombic signal for low-spin **2**$^{fac}$ and a low intensity signal for high-spin **2**$^{mer}$ emerge; similarly, the UV/Vis spectrum takes on characteristics of **2**$^{fac}$ and **2**$^{mer}$ (Figure S3 in the Supporting Information). This suggests either reversibility of PhIO binding [Eq. (2)] or that **3** has oxidized an unknown species in solution, with the concomitant regeneration of **2**. By using UV/Vis and ESR spectroscopy, we have also identified a transient 4-methyl-morpholine-*N*-oxide (NMO) adduct, [Fe$^{III}$(tpena)NMO]$^{2+}$ (**4**). Although rare, the oxidant NMO has been more often structurally characterized as a ligand in coordination compounds than PhIO.[18] However, none of these coordination compounds contain iron, which in fact has only rarely been observed to coordinate to aliphatic N-oxides.[19,20] When a slight excess of NMO is added to **2** in aprotic solutions, a subtle isobestic conversion takes place within approximately 17 s, forming the weakly yellow–red chromophore **4** (Figure 5 a). Complex **4** is more unstable at room temperature compared with **3** and decays within seconds to minutes to

ChemPubSoc Europe

CHEMISTRY
A European Journal
Full Paper



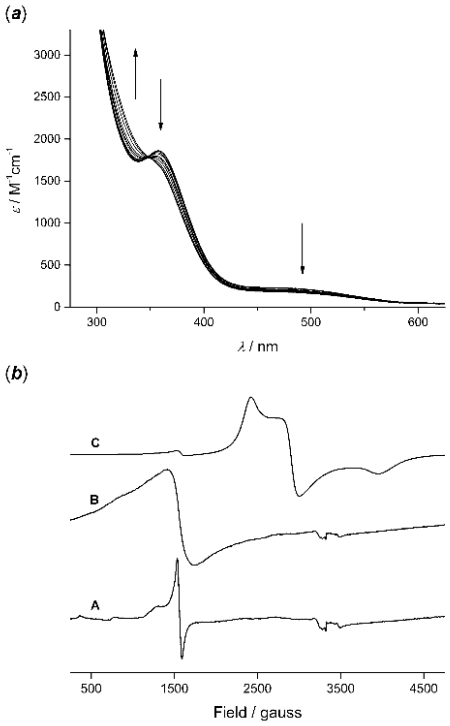


**Figure 5.** a) UV/Vis spectra showing the formation of **4** from 0.5 mM **2** and 2 equiv NMO in $CH_3CN$. Recorded over 18 s. b) ESR spectra (120 K in $CH_3CN$) of (C) **2** (5 mM), (B) **3** (5 mM, generated from mixing **2** and four equivalents PhIO), (A) **4** (5 mM, generated from mixing **2** and ten equivalents NMO). The weak signal observed around 3400 gauss is due to the coil of the thermal probe.

form **1**. We suggest that in contrast to **3**, the self-decay of **4** occurs by oxidation of a C–H bond in N-methylmorpholine. The outcome of this reaction will be the production of water. This will shift the equilibrium in Equation (1) towards **1**, and thereby inhibit subsequent NMO adduct formation owing to the diminishing concentrations of **2**. The decay can be slowed for several minutes if the solutions are cooled to −40 °C, enabling characterization by ESR spectroscopy (Figure 5b), which shows an axial signal with bands at $g_\perp = 4.00$ and $g_\parallel = 4.83$, consistent with high-spin **4**. The lower signal intensity in the spectrum of **4** compared with that of **3** is likely due to partial formation of ESR-silent **1**. All attempts to isolate **4** have resulted in the re-isolation of **1**.

### Catalytic oxidation of sulfides and olefins

In acetonitrile solutions, **2** catalyzes the oxidation of the electron-rich substrates thioanisole, diphenyl sulfide, and dibenzothiophene to the derived sulfoxides, as well as catalyzing conversion of *trans*-stilbene, cyclooctene, *n*-octene, *n*-decene to the derived epoxides by using both PhIO and NMO as terminal oxidants (Table 3). No diol formation was observed in the olefin epoxidations. An exclusively sulfoxidized product is obtained for the bifunctional substrate allyl phenyl sulfide, suggesting that sulfoxidation is easier than epoxidation. Of particular note is the swiftness and yield for the selective oxygenation of thioanisole. However, small amounts of the corresponding sulfones were produced with the diphenyl sulfide, dibenzothiophene, and allyl phenyl sulfide substrates. One explanation for this difference in selectivity is the difference in the reaction times required. The initial oxygenation of thioanisole to methyl phenyl sulfoxide proceeds much more readily than the initial sulfoxidation of dibenzothiophene to dithiophene sulfoxide; by contrast, the corresponding oxygenations of methyl phenyl sulfoxide and dibenzothiophene sulfoxide to their sulfones proceed at similar rates.[21] Overlap with the second oxygenation can occur during the prolonged time required for the initial monooxygenation of dibenzothiophene.

### Is the metal-based oxidant an iron(III)–OIPh/iron(III)–NMO or an iron(V)oxo species?

The selective and catalytic oxygenations of electron-rich substrates described above occur through either a direct oxygen atom transfer or by coupled electron transfer–oxygen transfer from **3**, **4**, or an iron(V)oxo species derived from heterolytic I–O or N–O cleavage in these oxidant adducts. The alternative mechanism involving homolytic FeO–X (X = IPh or N of NMO) cleavage products, an iron(IV)oxo species and/or the sister PhI$^{\bullet}$ or *N*-methylmorphyline$^{\bullet}$, which in turn activate an abundant O donor, for example, water, can be disregarded for two reasons: the absence of diol and carbonyl byproducts in the olefin epoxidations, and more indirectly by the lack of any spectroscopic detection of the green iron(IV)oxo derivative, $[Fe^{IV}O(tpenaH)]^{2-}$[16] or PhI$^{\bullet}$ radicals. Moreover, as an aggressive hydrogen atom abstractor, $[Fe^{IV}O(tpenaH)]^{2+}$ is a promiscuous oxidant and the presence of this species would result in many side-products, which, as stated, is not observed.

When acetonitrile solutions of **3** are treated with one equivalent of thioanisole at room temperature, the broad visible absorption at $\lambda = 428$ nm decays immediately in an exponential fashion, leading to a 240-fold reduction in its half-life from 4.6 h to 69 s. The reaction rate is even higher when higher concentrations of thioanisole are used. A second-order rate constant of $k_2 = 16.7 \times 10^{3}\ s^{-1}\ M^{-1}$ was determined (Figure 6a). ESR spectra show that **3** converts cleanly into **2**. During this time, a transient high-spin species, which we speculate could be an iron(III)–sulfoxide adduct, $[Fe(tpena)OS(CH_3)Ph]^{2+}$, is detected (Figure S8 in the Supporting Information). This is supported by the generation of the same ESR signal when **2** is treated with methyl phenyl sulfoxide.

Three direct metal-based oxidants are plausible: the detectable $[\mathbf{3}]_2$, an undetectable monomeric **3**, or an iron(V)oxo species derived from heterolytic I–O cleavage. If it is monomeric **3** or $[Fe^{V}O(tpena)]^{2+}$, it must react immediately after being formed, eliminating any concentration build-ups. Likewise, to account for the strong dependence of the rate on the substrate concentrations, $[Fe^{V}O(tpena)]^{2+}$ would need to be

ChemPubSoc Europe

CHEMISTRY A European Journal Full Paper

**Table 3.** Oxidative catalysis by **2** using PhIO and NMO as terminal oxidants.[a]

| Substrate | Oxidant | Oxidant loading [mol equiv] | Catalyst loading [mol%] | Reaction time [h] | Product | Yield [mol%] | TON[b] |
|---|---|---|---|---|---|---|---|
|  | PhIO | 1.1 | 0.1 | 1 | sulfoxide/sulfone | 80/0 | 800 |
| | NMO | 2.1 | 4.0 | 20 | | 69/0 | 20 |
| 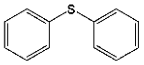 | PhIO | 1.1 | 1.0 | 3 | sulfoxide/sulfone | 78/9 | 87 |
| 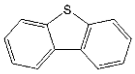 | PhIO | 1.1 | 1.0 | 5 | sulfoxide/sulfone | 54/16 | 70 |
| 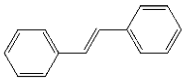 | PhIO | 1.1 | 1.0 | 16 | epoxide/diol | 95/0 | 95 |
| | NMO | 2.1 | 3.0 | 20 | | 80/0 | 27 |
| 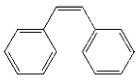 | PhIO | 1.1 | 1.0 | 5 | epoxide/diol | 14[c]/0 | 14 |
| | NMO | 2.1 | 3.0 | 20 | | 0/0 | 0 |
|  | PhIO | 1.1 | 1.0 | 20 | epoxide/diol | 10/0 | 10 |
| | NMO | 2.1 | 3.0 | 20 | | 3/0 | 1 |
| 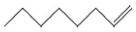 | PhIO | 1.1 | 1.0 | 8 | epoxide/diol | 79/0 | 79 |
|  | PhIO | 1.1 | 1.0 | 8 | epoxide/diol | 18/0 | 18 |
| 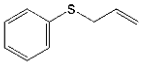 | PhIO | 1.1 | 1.0 | 1 | sulfoxide/sulfone[d] | 86/7 | 93 |

[a] Reactions performed under nitrogen at 50 °C with 150 mM substrate and 0.15–6 mM **2** in $CH_3CN$. [b] TON = turnover number. [c] Product distributed as 2% *cis*-stilbene oxide and 12% *trans*-stilbene oxide. [d] No epoxide products detected.

formed in a reversible reaction with **3** and PhI. As detailed by Hong et al. in a recent communication,[8c] if the formation is reversible the rate should be markedly slowed down by the presence of excess PhI. We observed no significant changes in the rate of thioanisole oxidation in the presence of 10–100 equivalents of PhI (Figure S13 in the Supporting Information). This implies that an iron–OIPh adduct is the metal-based oxidant. Confirming the notion that it is a very electrophilic oxidant, reactions of **3** with 4-methoxythioanisole are greatly accelerated, whilst the reaction with 4-(methylthio)benzonitrile is much slower (Table S4 in the Supporting Information). When correlating the second-order rate constants ($k_x$) with the electrophilic constants ($\sigma^+$), a large negative Hammett parameter of $\rho = -2.20$ is obtained (Figure 6b). The $\rho$ value is almost twice as large as those commonly observed for iron(IV)oxo species, and is much more in the range of those measured for iron(III)–OIPh[8(c)] and iron(IV)–tosylamido[22] adducts (Table S5 in the Supporting Information). Likewise, when the rate constants are correlated with the formal oxidation potentials of the sulfides, a Marcus-type plot is obtained with a large negative slope of $-6.56\ V^{-1}$ (Figure 6c). The value reflects the degree of electron transfer in the transition state, with the theoretical maximum for a pure electron-transfer process being $16.9\ V^{-1}$.[23] The large slope thus indicates that the oxidations proceed through a reaction that has more character of a coupled electron transfer–oxygen transfer process than a oxygen atom transfer, per se.[24,26]

Based on the mechanistic studies, we conclude that the evidence is overwhelmingly in favor of the active metal-based oxidant being an iron(III)–oxidant adduct and not a derived high-valent iron–oxo intermediate. Scheme 1 shows a proposed catalytic cycle. In this, we suggest that a dimer of $\mathbf{2}^{mer}$ extracts two equivalents of PhIO from $[PhIO]_n$. Driving this reaction is the remarkable stability of $[\mathbf{3}]_2$, which can be regarded as a protected form of the even more reactive **3**. As described, iron(III) adducts of the oxygenated product are also briefly detected. Water inhibits the reaction by hydrating **2** to form the pro-catalyst oxo-bridged complex **1**.

### Gas-phase studies

By obtaining a nanoelectrospray ionization (nESI) mass spectrum immediately after dissolving $\mathbf{3}(ClO_4)_2$ in acetonitrile at −4 °C, ions corresponding to $[\mathbf{3}\cdot ClO_4]^+$ ($m/z = 765$), $[\mathbf{3}\cdot Cl]^+$ ($m/z = 701$), and $[\mathbf{3}]^{2+}$ ($m/z = 333$) were detected (Figure 7). The stoichiometry of all the PhIO adduct ions were confirmed by accurate mass measurements performed on a Fourier transform ion cyclotron resonance mass spectrometer (<1 ppm mass accuracy). In addition, ions originating from the unavoidable hydrolysis of **2** and **3** corresponding to $[Fe_2O(tpena)_2]^{2+}$ ($[1-2H]^+$, $m/z = 454$), $[Fe^{III}(tpena)OH]^+$ ($m/z = 463$), $[Fe^{II}(tpena)]^-$ ($m/z = 446$), and the ferryl $[Fe^{IV}O(tpena)]^-$ ($m/z = 462$) were also formed. ESI-MS of $\mathbf{1}(ClO_4)_4$ and $\mathbf{2}(ClO_4)_2$ resulted in the formation and detection of the same ions ($m/z = 454$, 463, 446, and 462).

$[Fe_2O(tpena)_2]^{2+}$ and $[Fe^{III}(tpena)OH]^+$ can be expected to be generated from solutions of **1**.[16] Further collision-induced dissociation (CID) experiments performed on $[Fe^{III}_2O(tpena)_2]^{2+}$ to investigate the source of $[Fe^{II}(tpena)]^-$ and $[Fe^{IV}O(tpena)]^-$ (Figure S12 in the Supporting Information) show that they are formed by a gas-phase disproportionation[25] of this ion. Crucially, they are not derived from the solution state. CID of $[Fe^{III}_2O(tpena)_2]^{2+}$ also results in the generation of $[Fe^{III}(tpena)OH]^+$ and most of the degradation products observed in the ESI mass spectra of $1(ClO_4)_4$, including those at $m/z = 418$ ($[Fe(tpena\text{-}CO_2)]^+$), 388 ($[Fe(tpena\text{-}CH_2CO_2)]^+$), and 355 ($[Fe(tpena\text{-}CHPy)]^+$). CID of the species at $m/z = 462$ ($[Fe^{IV}O(tpena)]^-$) reveals that these product ions ($m/z = 418$, 388, and 355) can result from its intramolecular gas-phase oxi-

ChemPubSoc Europe

CHEMISTRY A European Journal Full Paper



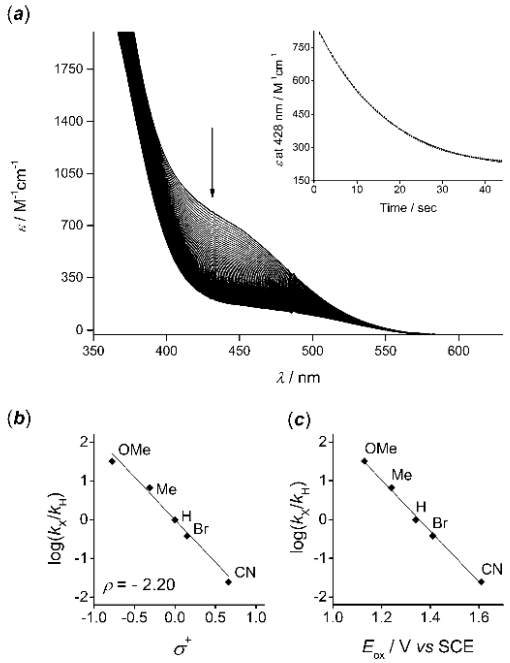


**Figure 6.** Kinetics of the reaction of **3** with *para*-substituted thioanisoles. a) Time-resolved UV/Vis spectra of the reaction of **3** with four equivalents of thioanisole. The insert shows the time trace at $\lambda = 428$ nm and its exponential fitting to extract the pseudo-first-order rate constant. b) Hammett plot of the logarithm of the second-order rate constants, $k_x$, versus the electrophilic constants[23] ($\rho = -2.20$, $R^2 = 0.994$). c) Marcus plot of $\log(k_x/k_H)$ versus the oxidation potentials of the *para*-substituted thioanisoles (slope $= -6.56\ V^{-1}$, $R^2 = 0.998$).

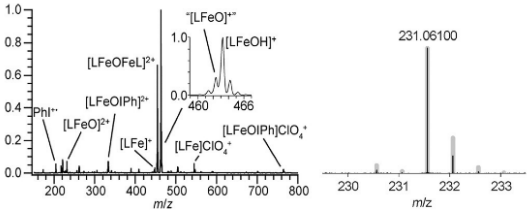


**Figure 7.** Left: nESI mass spectrum of **3**$(ClO_4)_2$ dissolved in $CH_3CN$. L = tpena$^-$. Right: High-resolution mass spectrum of the "$[Fe^{V}O(tpena)]^{2+}$" ion (black line) with its theoretical isotope pattern (thick gray line). The spectrum was obtained under conditions most optimal for detecting $\mathbf{3}^{2+}$. By contrast, most spectra (but not actually this spectrum) show its anion adducts [**3**·$ClO_4$]$^+$ and [**3**·Cl]$^+$ with a greater ion intensity (for example, see Figure S10 in the Supporting Information).

dative decomposition. The sequential decomposition reactions of $[Fe^{III}_2O(tpena)_2]^{2+}$ and $[Fe^{IV}O(tpena)]^+$ are shown in Equations (3) and (3a).

Ions ostensibly corresponding to $[Fe^{IV}O(tpena)]^+$ ($m/z = 462$), "$[Fe^{V}O(tpena)]^{2+}$" ($m/z = 231$), and $[PhI]^{\bullet+}$ ($m/z = 204$) found in the spectrum of **3**$(ClO_4)_2$ are particularly interesting (Figure 7).

$$[Fe^{III}_2O(tpena)_2]^{2+} \xrightarrow{CID} [Fe^{IV}O(tpena)]^+ + [Fe^{II}(tpena)]^+ \quad Eq.\ 3$$
($m/z$ 454.1) ($m/z$ 462.1) ($m/z$ 446.1)

$$[Fe^{IV}O(tpena)]^+ \xrightarrow{CID} [Fe^{II}(tpena\text{-}CHpy)]^+ + [picolinic\ aldehyde] \quad Eq.\ 3a$$
($m/z$ 462.1) ($m/z$ 355.1) (*proposed neutral fragment*)

Only on rare occasions was the dicationic **3** directly observed. Isolation and storage of **3** for 10 s (with no intentional deposition of internal energy into the ion through CID) resulted in spontaneous coulombic fission to form the ions corresponding to $[Fe^{IV}O(tpena)]^+$ and $PhI^{\bullet+}$. This amounts to a facile gas-phase homolysis of the O–I bond of the doubly charged precursor ion [Eq. (4), Figure S11 in the Supporting Information]. In contrast, [**3**·$ClO_4$)]$^+$ is highly stable with respect to dissociation when isolated and can be stored for up to 10 s. A CID mass spectrum of the anion adduct is shown in Figure S11 b. Upon CID, this ion dissociates through the loss of $PhIClO_4$ and $HClO_4$ to form $[Fe^{IV}O(tpena)]^+$ and $[Fe(tpena\text{-}H)OIPh]^+$, respectively [Eqs. (5) and (6)]. To summarize, the dicationic $[Fe(tpena)OIPh]^{2+}$ ion (**3**) decays significantly faster than its anion adducts. Also consistent is the fact that $[Fe(tpena)OIPh]^{2+}$ is detected in comparatively low abundance compared with the anion adducts. Overall, these data suggest a structurally stabilizing interaction between $[\mathbf{3}]^{2-}$ and $ClO_4^-$ (and adventitious $Cl^-$) in the gas phase. It seems unlikely that the anions should be directly coordinated to the metal center to form an octadentate coordination complex. Thus, we hypothesize that the anions and $[\mathbf{3}]^{2+}$ interact through halogen-bonding I···$OClO_3$ or I···Cl interactions. This is in line with the observations of Wang et al.,[18i–j] who have recently structurally characterized [Mn(salen){(OI(Cl)(Ph)}$_2$]. In this complex, the chloride atoms can be regarded as bonded to the iodine atom of the PhIO unit (average I–Cl, 2.675 Å).

$$[\mathbf{3}]^{2+} \longrightarrow [Fe^{IV}O(tpena)]^+ + [PhI^{\bullet}]^+ \quad Eq.\ 4$$
($m/z$ 333.0) ($m/z$ 462.1) ($m/z$ 204.0)

$$[\mathbf{3}.ClO_4]^+ \xrightarrow{CID} [Fe^{IV}O(tpena)]^+ + [PhIClO_4] \quad Eq.\ 5$$
($m/z$ 765.0) ($m/z$ 462.1) (*proposed neutral fragment*)

$$[\mathbf{3}.ClO_4]^+ \xrightarrow{CID} [Fe^{II}(tpena\text{-}H)(OIPh)]^+ + [HClO_4] \quad Eq.\ 6$$
($m/z$ 765.0) ($m/z$ 665.0) (*proposed neutral fragment*)

$$[Fe^{II}(tpena\text{-}H)(OIPh)]^+ \xrightarrow{CID} [Fe^{II}(tpena\text{-}H)]^+ + [OIPh] \quad Eq.\ 6a$$
($m/z$ 665.0) ($m/z$ 545.1) (*proposed neutral fragment*)

With reference to the above analyses of the ESI and CID mass spectra of **1**$(ClO_4)_4$, **2**$(ClO_4)_2$, and **3**$(ClO_4)_2$, and consideration of the gas- versus solution-phase sources of ions, it was noteworthy that a low abundance ion with an accurate mass value of $m/z = 231.06100$ (versus the theoretical value 231.06088 for $\{Fe(tpena) + O\}^{2+}$) in Figure 7 (right) appeared

ChemPubSoc Europe

CHEMISTRY A European Journal Full Paper

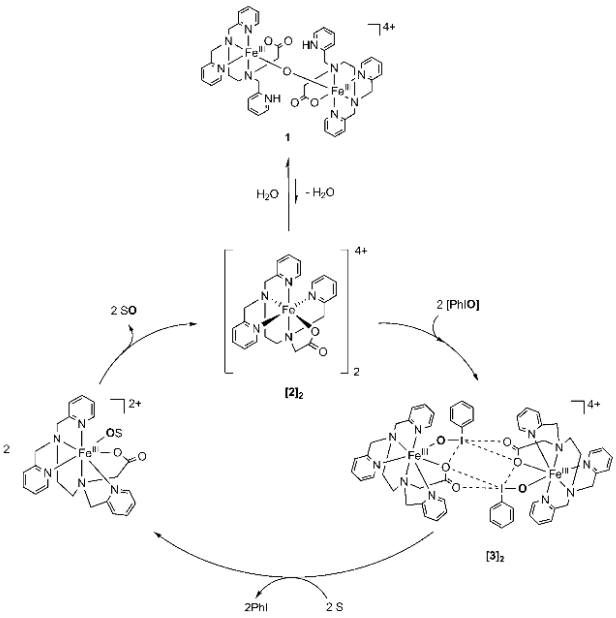


**Scheme 1.** A proposed mechanism in which $[\mathbf{2}]_2$ solubilizes $[PhIO]_n$ to form $[\mathbf{3}]_2$. All the structurally characterized $[Fe(tpena)]^{2+}$ species (**1**, $[\mathbf{2}^{fac}]_2$, $[\mathbf{3}]_2$) occur as dimers or in the case of the pro-catalyst as an oxo-bridged complex, suggesting that pairs of complexes work in unison to mobilize $[PhIO]_n$.

*only* in the spectra of $\mathbf{3}(ClO_4)_2$: thus, crucially, it cannot be "synthesized" in the gas phase, for example by the CID of any of $[\mathbf{3}]^{2+}$, $[\mathbf{3}{\cdot}A]^+$ ($A = ClO_4^-$, $Cl^-$), $[Fe_2O(tpena)_2]^{2+}$, or $[Fe^{IV}O(tpena)]^+$ species. Although this $m/z = 231$ ion is consistent with the formulation for the elusive $[Fe^{V}O(tpena)]^{2+}$ species (Figure 8 A), alternative structural formulations are plausible. In these, the ligand is oxygenated and the formula is better represented by "$[Fe^{III}(tpenaO)]^{2+}$" (Figure 8 B–D). There is precedence for both in situ N-donors and aromatic oxygenations in iron complexes of a pentadentate N4O ligand related to tpena$^-$ by replacement of a methylpyridyl group with a methyl group,[20] and peracid complexes have been identified.[27] Although inconclusive, the lack of reactivity of the $m/z = 231$ ion towards potentially oxidizable gas-phase substrates (MeOH, EtOH, $CH_4$, and $(CH_3)_2S$) in attempted gas-phase ion–molecule reactions (IMRs) point to the $[Fe^{III}(tpenaO)]^{2+}$ formulations as we anticipate that a perferryl species would oxidize these substrates. It is relevant to note that this IMR technique was successfully implemented for the gas-phase oxidation of alcohols by using a $S = 2$ iron(IV)oxo species.[28]

## Conclusion

We have shown that the iron(III) complex of the potentially hexadentate ligand tpena$^-$ is capable of activating the oxidants PhIO and NMO through formation of seven-coordinated iron(III)–oxidant adducts. Hexadenticity for ligands supporting catalysts is unusual as they are typically regarded as "saturating", particularly for first row metal ions. This might be true for the crystallographically characterized low-spin $\mathbf{2}^{fac}$ diastereoisomer of $[Fe^{III}(tpena)]^{2-}$ and that it is the presumably more reactive high-spin diastereoisomer $\mathbf{2}^{mer}$ that can more readily expand its coordination number and bind the O-donor oxidants. In the catalytic oxidation of aromatic sulfides and olefins the unanticipated stability of the iron(III)–OIPh adduct, $[Fe^{III}(tpena)OIPh]^{2+}$ (**3**), compared with the analogous iron(III)–NMO adduct, $[Fe^{III}(tpena)(NMO)]^{2-}$ (**4**), is presumably important for rendering the former a superior catalytic oxidizing system. Kinetic studies and a correlation of the rates of the reaction of **3** with a series *para*-substituted thioanisoles suggest that the direct oxidants in the catalytic reactions are iron(III)–OIPh species. An elegant duet by pairs of $[Fe^{III}(tpena)]^{2}$ complexes effects the solubilization of insoluble PhIO by coordination and concomitant self-protection to produce higher concentrations of the active oxidizing species. Our hypothesis was that homogeneity would effect more efficient catalytic oxidations by using NMO as the terminal oxidant compared with those using highly insoluble PhIO, for which reactions are by necessity heterogeneous. This proved not to be the case and the decreased solution-state stability of **4** compared with **3** can be correlated with the lower effectivity.

The observations provide an interesting example of halogen-bonding being strong enough in solution to be useful in assisting in homogeneous catalysis. Evidence for supramolec-

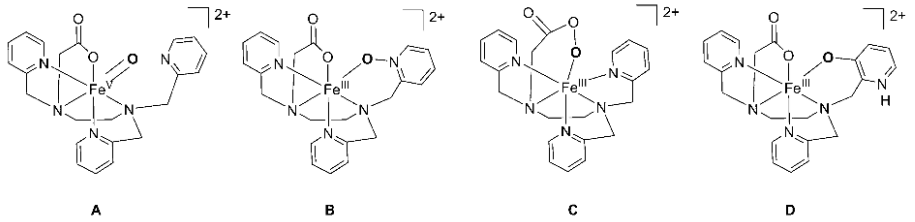


**Figure 8.** Structural assignments for the $m/z = 231.06100$ ion: a perferryl complex (**A**) and isobaric isomers of $[Fe^{II}(tpenaO)]^{2}$ with variously oxygenated tpena$^-$ ligands (**B–D**).

ChemPubSoc Europe

CHEMISTRY A European Journal Full Paper



ular halogen-bonding interactions between the I atom of the coordinated PhIO and the electron-donating carbonyl groups of another cation in dimeric structures or anions was found in the solid, solution, and gas phases. Noteworthy is the quenching of the otherwise strong carboxylato bands in the IR spectra of **3**$(ClO_4)_2$ caused by the symmetry imposed by the halogen-bonded dimers. It is possible that potentially characteristic metal–OIPh vibrations have been quenched by the same structural features.

Through a series of CID and IMR experiments, we have established that $[Fe^{IV}O(tpena)]^+$ is formed by gas-phase reaction only; there is no evidence for the presence of this species, and hence its participation, in the solution-phase catalysis reactions. Notably, an ion that might have been mistakenly assigned to the perferryl $[Fe^{V}O(tpena)]^{2+}$ is ascertained to be derived from solutions containing the PhIO adduct **3**. The same ion could not be generated in the gas-phase reaction. The lack of gas-phase reactivity observed for this ion suggests that it is more likely to be an iron(III) complex of oxygenated tpena$^-$.

## Experimental Section

### Materials

Commercially available reagents were purchased from Sigma–Aldrich and used without further purification. Acetonitrile and diethyl ether were dried over activated 3 Å molecular sieves. PhIO,[29] $[Fe_2O(tpenaH)_2](ClO_4)_4(H_2O)_2$ (**1**$(ClO_4)_4$),[2] and $[Fe(tpena)OIPh](ClO_4)_2$-$(CH_3CN)(H_2O)_{0.5}$ (**3**$(ClO_4)_4$)[2] were prepared as previously described.

***Caution!*** Perchlorate salts are potentially explosive upon exposure to excess heat or shock, and should be handled with care and only in small quantities.

### Instrumentation

$^1$H NMR spectra were recorded on a Bruker AVANCE III 400 spectrometer. Gas chromatographic analyses were performed on an HP 6890 Series GC system equipped with a Carbowax/20 m polyethylene glycol capillary column and flame ionization detector. GC-MS analyses were performed on a Bruker 451-GC SCION SQ MS equipped with a ZB WAX 624 column. ATR-IR spectra were recorded as neat solids on a PerkinElmer Spectrum Two spectrometer. All spectra have been ATR- and baseline corrected. UV/Vis spectra were recorded on an Agilent 8453 spectrophotometer using 1 cm quartz cuvettes. ESR spectra where recorded on a Bruker EMX Plus CW spectrometer. Mössbauer spectra were obtained with conventional constant acceleration spectrometers with sources of $^{57}$Co in rhodium. The spectrometers were calibrated by using a 12.5 μm foil of α-Fe. Spectra were obtained at 18–150 K by using a closed cycle helium refrigerator from APD Cryogenics. Powdered samples were contained in plastic holders (16 mm in diameter). ESI-MS spectra were recorded on either a nanospray Finnigan hybrid linear quadrupole ion trap and a 7 T Fourier transform ion cyclotron resonance (FT/ICR) mass spectrometer, or a nanospray orbitrap XL mass spectrometer.

### [Fe(tpena)]$(ClO_4)_2$-2$(ClO_4)_2$

Diethyl ether was added at −40 °C into solutions of **1**$(ClO_4)_4$ dissolved in dry acetonitrile (5 mM); the solutions were allowed to stand for 30 min before cooling. Solid pale or orange powders were isolated. If diethyl ether was diffused into the solution, red–orange crystals of **2**$^{fac}(ClO_4)_2$·1.5 $CH_3CN$ were deposited along with brown crystals of **1**$(ClO_4)_4$. Elemental analysis calcd (%) for **2**$(ClO_4)_2$·$H_2O$ ($FeC_{22}H_{26}Cl_2N_5O_{11}$): C 39.85, H 3.95, N 10.56.; found: C 39.58, H 3.87, N, 10.31.

### PhI$^{18}$O

Small well-polished cubes of sodium (69 mg, 3 mmol) were slowly added over 30 min to ice-cold $H_2{}^{18}O$ (1000 μL) with stirring and under $N_2$. After this time, finely ground vacuum-dried PhI$(OAc)_2$ (150 mg, 0.47 mmol) was carefully added. Rigorous stirring under $N_2$ was continued for 3 h. Solids sticking to the sides of the flask were washed down with 300 μL $H_2{}^{18}O$. Initially, the solid sticks to the magnet, but as the color changes from white to creamy yellow a much more homogeneous dispersion was obtained. The dispersion was carefully transferred to a centrifuge glass and centrifuged. The isolated liquor was used to extract the last of the solid from the reaction flask. The isolated solid was washed with unlabeled water (until pH neutral), then with acetonitrile, and finally diethyl ether. The pale-yellow solid was dried under vacuum for 17 h and stored at −40 °C.

### Other $^{18}$O-labeled species

$[Fe(tpena)^{18}OIPh](ClO_4)_2$ was prepared similarly to its unlabeled counterpart[2] by the in situ dehydration of **1**$(ClO_4)_4$ in dry acetonitrile over 30 min, followed by the addition of excess PhI$^{18}$O, filtration, and precipitation of the product at −40 °C by diethyl ether. $[Fe_2{}^{18}O(tpenaH)_2](ClO_4)_2$ was prepared by recrystallizing **1**$(ClO_4)_4$ from 95% $H_2{}^{18}O$.

$^{18}$O-methyl phenyl sulfoxide was prepared by either a direct reaction of thioanisole with $^{18}$O-**3**$(ClO_4)$ or by first exposing **3**$(ClO_4)_2$ (1.8 mg, 2 μmol) in dry acetonitrile (200 μL) to 95% $H_2{}^{18}O$ (250 equiv, 9 μL) for 20 s and then adding 1 equiv neat thioanisole. The solution was allowed to stand for 5 min at RT. After dilution, the sample was analyzed by GC-MS, which showed a 91% yield (Figure S9 in the Supporting Information).

### Catalysis and kinetic experiments

The substrate (0.9 mmol) and oxidant (1.1 equiv, PhIO or NMO) were dispersed in dry acetonitrile (4 mL). **2** (0.05–4 mol%) was added as an aliquot from a 10 mM acetonitrile stock solution. The reaction mixture was lowered into a pre-heated oil bath at 50 °C and stirred under nitrogen for the prescribed amount of time. The cooled solution was gravity filtered and divided between diethyl ether (or dichloromethane, 15 mL) and water (2 mL). The organic phase was evaporated in vacuo to yield the crude product. Depending on the boiling point of the substrate, product analysis was performed by GC by using biphenyl as internal standard or by $^1$H NMR spectroscopy in $CDCl_3$ (or $CD_3CN$). It was found that the catalyst could be recovered intact as **1**$(ClO_4)_4$ (as judged by IR and ESI-MS) by pooling the aqueous phases from several experiments and evaporating them in vacuo. The resulting brown oils solidified upon exposure to a small amount of 96% aqueous ethanol.

Kinetic experiments were carried out at 19–22 °C. Complex **3** (2000 μL, 1 mM, 2 μmol), taken from a freshly prepared 1 mM stock of **3**$(ClO_4)_2$ (1.8–2.4 mg) dissolved in the appropriate amount of acetonitrile, was transferred to a cuvette. Whilst measuring the UV/Vis spectrum of the solution, an aliquot from a 40 mM stock (5–15 μmol) of the appropriate *para*-substituted phenyl methyl sulfide was added quickly, and the change in the spectra was monitored as a function of time. Pseudo-first-order rate constants, $k_{obs}$, were

 

ChemPubSoc Europe

CHEMISTRY A European Journal Full Paper

extracted by exponential fitting of the extinction at $\lambda = 428$ nm using the Agilent ChemStation software (Levenberg–Marquardt algorithm). The second-order rate constant, $k$, was extracted by linear regression of a plot of $k_{obs}$ values against the substrate concentration. Selected samples were evaporated in vacuo and subjected to $^1$H NMR spectroscopic analysis in $CDCl_3$ to confirm that the corresponding sulfoxides had formed.

### Supporting Information

Details of structure determinations, UV/Vis monitoring of formation and decays of reactive species, IR spectra of $^{18}$O-labeled compounds, and ESR spectra, ESI and CID mass spectra are given along with details of the kinetic analyses. CCDC 1414517 contains the supplementary crystallographic data for this paper. These data are provided free of charge by The Cambridge Crystallographic Data Centre.

## Acknowledgement

This work was supported by the Danish Council for Independent Research | Natural Sciences (grant 12-124985 to C.McK.) and the University of Southern Denmark. We thank Dr. Simon Svane for help with ESI-MS. The COST CM1003 action is acknowledged for travel funding.

**Keywords:** epoxidation · gas-phase chemistry · halogen-bonding · iodosylbenzene · iron · sulfoxidation

[1] D. Macikenas, E. Skrzypczak-Jankun, J. D. Protasiewicz, *J. Am. Chem. Soc.* **1999**, *121*, 7164–7165.

[2] A. Lennartson, C. J. McKenzie, *Angew. Chem. Int. Ed.* **2012**, *51*, 6767–6770; *Angew. Chem.* **2012**, *124*, 6871–6874.

[3] a) A. R. McDonald, L. Que, Jr., *Coord. Chem. Rev.* **2013**, *257*, 414–428; b) S. Hong, Y.-M. Lee, W. Shin, S. Fukuzumi, W. Nam, *J. Am. Chem. Soc.* **2009**, *131*, 13910–13911; c) A. Mukherjee, M. A. Cranswick, M. Chakrabarti, T. K. Paine, K. Fujisawa, E. Münck, L. Que, Jr., *Inorg. Chem.* **2010**, *49*, 3618–3628; d) Y.-M. Lee, S. Hong, Y. Morimoto, W. Shin, S. Fukuzumi, W. Nam, *J. Am. Chem. Soc.* **2010**, *132*, 10668–10670; e) M. M. Mbughuni, M. Chakrabarti, J. A. Hayden, E. L. Bominaar, M. P. Hendrich, E. Munck, J. D. Lipscomb, *Proc. Natl. Acad. Sci. USA* **2010**, *107*, 16788–16793; f) S. Chatterjee, D. Sheet, T. K. Paine, *Chem. Commun.* **2013**, *49*, 10251–10253; g) C.-W. Chiang, S. T. Kleespies, H. D. Stout, K. K. Meier, P.-Y. Li, E. L. Bominaar, L. Que, Jr., E. Münck, W.-Z. Lee, *J. Am. Chem. Soc.* **2014**, *136*, 10846–10849; h) B. Chakraborty, S. Bhunya, A. Paul, T. K. Paine, *Inorg. Chem.* **2014**, *53*, 4899–4912.

[4] a) K. B. Jensen, C. J. McKenzie, L. P. Nielsen, J. Z. Pedersen, H. M. Svendsen, *Chem. Commun.* **1999**, 1313–1314; b) J. Annaraj, Y. Suh, M. S. Seo, S. O. Kim, W. Nam, *Chem. Commun.* **2005**, 4529–4531; c) J. Cho, S. Jeon, S. A. Wilson, L. V. Liu, E. A. Kang, J. J. Braymer, M. H. Lim, B. Hedman, K. O. Hodgson, J. S. Valentine, E. I. Solomon, W. Nam, *Nature* **2011**, *478*, 502–505; d) Y.-M. Lee, S. Bang, Y. M. Kim, J. Cho, S. Hong, T. Nomura, T. Ogura, O. Troeppner, I. Ivanović-Burmazović, R. Sarangi, S. Fukuzumi, W. Nam, *Chem. Sci.* **2013**, *4*, 3917–3923.

[5] a) I. Bernal, I. M. Jensen, K. B. Jensen, C. J. McKenzie, H. Toftlund, J. P. Tuchagues, *J. Chem. Soc. Dalton Trans.* **1995**, 3667–3675; b) A. Wada, S. Ogo, S. Nagatomo, T. Kitagawa, Y. Watanabe, K. Jitsukawa, H. Masuda, *Inorg. Chem.* **2002**, *41*, 616–618; c) S. Taktak, M. Flook, B. M. Foxman, L. Que, Jr., E. V. Rybak-Akimova, *Chem. Commun.* **2005**, 5301–5303; d) O. V. Makhlynets, P. Das, S. Taktak, M. Flook, R. Mas-Ballesté, E. V. Rybak-Akimova, L. Que, Jr., *Chem. Eur. J.* **2009**, *15*, 13171–13180; e) A. Thibon, V. Jollet, C. Ribal, K. Senechal-David, L. Billon, A. B. Sorokin, F. Banse, *Chem. Eur. J.* **2012**, *18*, 2715–2724.

[6] J. Kim, E. Larka, E. C. Wilkinson, L. Que, Jr., *Angew. Chem. Int. Ed. Engl.* **1995**, *34*, 2048–2051; *Angew. Chem.* **1995**, *107*, 2191–2194.

[7] A. Draksharapu, D. Angelone, M. G. Quesne, S. K. Padamati, L. Gýmez, R. Hage, M. Costas, W. R. Browne, S. P. de Visser, *Angew. Chem. Int. Ed.* **2015**, *54*, 4357–4361; *Angew. Chem.* **2015**, *127*, 4431–4435.

[8] a) J. P. Collman, A. S. Chien, T. A. Eberspacher, M. Zhong, J. I. Brauman, *Inorg. Chem.* **2000**, *39*, 4625–4629; b) K. P. Bryliakov, E. P. Talsi, *Chem. Eur. J.* **2007**, *13*, 8045–8050; c) S. Hong, B. Wang, M. S. Seo, Y.-M. Lee, M. J. Kim, H. R. Kim, T. Ogura, R. Garcia-Serres, M. Clémancey, J.-M. Latour, W. Nam, *Angew. Chem. Int. Ed.* **2014**, *53*, 6388–6392; *Angew. Chem.* **2014**, *126*, 6506–6510; d) K. P. Bryliakov, D. E. Babushkin, E. P. Talsi, *Mendeleev Commun.* **2000**, *10*, 1–3; e) Y. Yang, F. Diederich, J. S. Valentine, *J. Am. Chem. Soc.* **1990**, *112*, 7826–7828; f) K. P. Bryliakov, D. E. Babushkin, E. P. Talsi, *J. Mol. Catal. A* **2000**, *158*, 19–35; g) K. P. Bryliakov, E. P. Talsi, *Angew. Chem. Int. Ed.* **2004**, *43*, 5228–5230; *Angew. Chem.* **2004**, *116*, 5340–5342; h) C. Wang, T. Kurahashi, H. Fujii, *Angew. Chem. Int. Ed.* **2012**, *51*, 7809–7811; *Angew. Chem.* **2012**, *124*, 7929–7931; i) C. Wang, T. Kurahashi, K. Inomata, M. Hada, H. Fujii, *Inorg. Chem.* **2013**, *52*, 9557–9566.

[9] N. Ortega-Villar, A. Y. Guerrero-Estrada, L. Piñeiro-López, M. C. Muñoz, M. Flores-Álamo, R. Moreno-Esparza, J. A. Real, V. M. Ugalde-Saldívar, *Inorg. Chem.* **2015**, *54*, 3413–3421.

[10] M. S. Vad, A. Nielsen, A. Lennartson, A. D. Bond, J. E. McGrady, C. J. McKenzie, *Dalton Trans.* **2011**, *40*, 10698–10707.

[11] D. P. de Sousa, J. Bigelow, J. Sundberg, L. Que, Jr., C. J. McKenzie, *Chem. Commun.* **2015**, *51*, 2802–2805.

[12] A. Bondi, *J. Phys. Chem.* **1964**, *68*, 441–451.

[13] R. Glaser, N. Chen, H. Wu, N. Knotts, M. Kaupp, *J. Am. Chem. Soc.* **2004**, *126*, 4412–4419.

[14] a) J.-U. Rohde, J.-H. In, M. H. Lim, W. W. Brennessel, M. R. Bukowski, A. Stubna, E. Münck, W. Nam, L. Que, Jr., *Science* **2003**, *299*, 1037–1039; b) W. J. Song, Y. J. Sun, S. K. Choi, W. Nam, *Chem. Eur. J.* **2006**, *12*, 130–137; c) J. T. Groves, W. J. Kruper, *J. Am. Chem. Soc.* **1979**, *101*, 7613–7615; d) F. F. Pfaff, S. Kundu, M. Risch, S. Pandian, F. Heims, I. Pryjomska-Ray, P. Haack, R. Metzinger, E. Bill, H. Dau, P. Comba, K. Ray, *Angew. Chem. Int. Ed.* **2011**, *50*, 1711–1715; *Angew. Chem.* **2011**, *123*, 1749–1753; e) S. H. L. Wang, B. S. Mandimutsira, R. Todd, B. Ramdhanie, J. P. Fox, D. P. Goldberg, *J. Am. Chem. Soc.* **2004**, *126*, 18–19; f) H. Kotani, S. Kaida, T. Ishizuka, M. Sakaguchi, T. Ogura, Y. Shiota, K. Yoshizawa, T. Kojima, *Chem. Sci.* **2015**, *6*, 945–955; g) J. England, J. O. Bigelow, K. M. Van Heuvelen, E. R. Farquhar, M. Martinho, K. K. Meier, J. R. Frisch, E. Münck, L. Que, Jr., *Chem. Sci.* **2014**, *5*, 1204–1215.

[15] Halogen-bonding does not quench carboxylate IR absorption bands *per se*. For example, the carboxylate bands are strong in the IR spectra of 2-iodobenzoic and 2-iodosobenzoic acid (IBX), both of which contain halogen-bonds (Figure S7 in the Supporting Information).

[16] M. S. Vad, A. Lennartson, A. Nielsen, J. Harmer, J. E. McGrady, C. Frandsen, S. Morup, C. J. McKenzie, *Chem. Commun.* **2012**, *48*, 10880–10882.

[17] a) H. H. Wickman, M. P. Klein, D. A. Shirley, *Phys. Rev.* **1966**, *152*, 345–357; b) M. Blume, J. A. Tjon, *Phys. Rev.* **1968**, *165*, 446–456; c) S. Mørup, in *Mössbauer Spectroscopy and Transition Metal Chemistry: Fundamentals and Applications* (Eds.: P. Gütlich, E. Bill, A. X. Trautwein), Springer, Berlin, pp. 201–34.

[18] The uncertainty of the isomer shifts, the quadrupole splittings, and the line widths of $\mathbf{1}(ClO_4)_4$ and $\mathbf{2}^{fac}(ClO_4)_2$ are about 0.02 mm s$^{-1}$. The uncertainties of the parameters of the broad singlets due to $\mathbf{2}^{mer}(ClO_4)_2$ and $\mathbf{3}(ClO_4)_2$ are somewhat larger. Therefore, the uncertainties of the relative areas of all components is also relatively large, of the order of 5–10%.

[19] a) A. J. Bailey, M. G. Bhowon, W. P. Griffith, A. G. F. Shoair, A. J. P. White, D. J. Williams, *J. Chem. Soc. Dalton Trans.* **1997**, 3245–3250; b) R. B. Brown, M. M. Williamson, C. L. Hill, *Inorg. Chem.* **1987**, *26*, 1602–1608.

[20] A. Nielsen, F. B. Larsen, A. D. Bond, C. J. McKenzie, *Angew. Chem. Int. Ed.* **2006**, *45*, 1602–1606; *Angew. Chem.* **2006**, *118*, 1632–1636.

[21] M. B. Chambers, S. Groysman, D. Villagrán, D. G. Nocera, *Inorg. Chem.* **2013**, *52*, 3159–3169.

[22] a) A. A. Humffray, H. E. Imberger, *J. Chem. Soc. Perkin Trans.* **1981**, *2*, 382–387; b) A. K. Vardhaman, S. Sikdar, C. V. Sastri, *Ind. J. Chem. Sect. A* **2011**, *50*, 427–431.

[23] a) H. C. Brown, Y. Okamoto, *J. Am. Chem. Soc.* **1958**, *80*, 4979–4987; b) Y. Goto, T. Matsui, S. Ozaki, Y. Watanabe, S. Fukuzumi, *J. Am. Chem. Soc.* **1999**, *121*, 9497–9502.

ChemPubSoc Europe

CHEMISTRY
A European Journal
Full Paper

[24] A. K. Vardhaman, P. Barman, S. Kumar, C. V. Sastri, D. Kumar, S. P. de Visser, *Angew. Chem. Int. Ed.* **2013**, *52*, 12288 – 12292; *Angew. Chem.* **2013**, *125*, 12514 – 12518.
[25] L. Eberson, *Electron Transfer Reactions in Organic Chemistry* (Eds.: K. Hafner, J.-M. Lehn, C. W. Rees, P. von Ragué Schleyer, B. M. Trost, R. Zahradník) *Reactivity and Structure Concepts in Organic Chemistry*, Springer Heidelberg, **1987**.
[26] J. Park, Y. Morimoto, Y.-M. Lee, W. Nam, S. Fukuzumi, *J. Am. Chem. Soc.* **2011**, *133*, 5236 – 5239.
[27] J. Nakazawa, S. Terada, M. Yamada, S. Hikichi, *J. Am. Chem. Soc.* **2013**, *135*, 6010 – 6013.
[28] W. A. Donald, C. J. McKenzie, R. A. J. O'Hair, *Angew. Chem. Int. Ed.* **2011**, *50*, 8379 – 8383; *Angew. Chem.* **2011**, *123*, 8529 – 8533.
[29] P. Dauban, L. Sanière, A. Tarrade, R. H. Dodd, *J. Am. Chem. Soc.* **2001**, *123*, 7707 – 7708.

Received: August 7, 2015
Revised: September 22, 2015
Published online on November 24, 2015

 